Optical Control of Solar Sails using Distributed Reflectivity

Andreas Borggräfe*
University of Strathclyde, Glasgow, G1 1XJ, United Kingdom

Jeannette Heiligers†
University of Strathclyde, Glasgow, G1 1XJ, United Kingdom

Matteo Ceriotti‡
University of Glasgow, Glasgow, G12 8QQ, United Kingdom

Colin R. McInnes§
University of Strathclyde, Glasgow,G1 1XJ, United Kingdom

The dynamics of solar sails with a variable surface reflectivity distribution are investigated. When changing the reflectivity across the sail film, which can be achieved using electro-chromic coatings, the solar radiation pressure forces and torques across the sail film can be controlled without changing the attitude of the spacecraft relative to the Sun and without using mechanical systems. The paper presents two approaches. First, a continuous reflectivity distribution is presented to control the sail attitude under the influence of, for example, gravity gradient torques in Earth orbit. The second approach assumes discrete on/off reflectivity regions across the surface. Both concepts of 'optical reconfiguration' of solar sails enable a more flexible steering of the spacecraft and minimize actuation effort.

I. Introduction

Using conventional solar sailing technology, the solar radiation pressure (SRP) force vector direction and magnitude depend strongly on the sail attitude relative to the Sun, limiting the applicability of solar sails compared to other low-thrust propulsion systems such as solar-electric propulsion. Furthermore, the SRP force magnitude follows an inverse square law with solar distance, making the sail less efficient at large distances from the Sun.[1] In order to increase the flexibility of modulating the SRP forces and torques, and to decrease the total mass of the spacecraft, we introduce the concept of variable optical properties for large gossamer spacecraft. In particular, the attitude dynamics of a rigid, flat solar sail with a variable surface reflectivity distribution are investigated. When changing the reflectivity coefficient across the sail film, the SRP forces and torques acting on the sail can be controlled without changing the incidence angle relative to the Sun and without using mechanical systems. The reflectivity can in principle be modified using electro-chromic coatings, which consist of an electro-active material that changes its surface reflectivity according to an applied electric potential.[2] By assigning an appropriate reflectivity distribution across the sail area, the center-of-pressure can be shifted optically relative to the center-of-mass (CoM), rather than mechanically, as for example through the use of moving payload masses.

*PhD Researcher, Department of Mechanical and Aerospace Engineering, 75 Montrose Street, James Weir Building, University of Strathclyde, Glasgow G1 1XJ, United Kingdom, AIAA Student Member.

†Research Associate, Department of Mechanical and Aerospace Engineering, 75 Montrose Street, James Weir Building, University of Strathclyde, Glasgow G1 1XJ, United Kingdom.

‡Lecturer, School of Engineering, James Watt South Building, University of Glasgow, G12 8QQ, United Kingdom, AIAA Member.

§Professor, Department of Mechanical and Aerospace Engineering, 75 Montrose Street, James Weir Building, University of Strathclyde, Glasgow, G1 1XJ, United Kingdom.

The paper will demonstrate the potential of using distributed reflectivity for optical control of the sail attitude. First, in section II, the reflectivity distribution $\rho(s)$ is ideally assumed to be continuous across the surface, with arbitrary values of ρ in the interval $[0, 1]$. Through this, the reflectivity can be modulated continuously between diffuse and specular reflection. The concept is applied to counteract gravity gradient torques in a planar Earth orbit. Subsequently, in section III, a more realistic approach is taken, using discrete regions of activated and deactivated (on/off) reflectivity, separated by a variable boundary line. When controlling the position of the boundary line across the surface, a wide range of torque vector directions in the sail-plane can be generated. This approach is demonstrated for two-axis attitude control of the sail in a Sun-centered orbit. It will be shown that through a basic maneuver about two axes, the sail can be brought to a Sun-pointing attitude from a chosen initial displacement. Since the SRP forces acting on the sail vary with the sail's attitude with respect to the Sun, an analytic method will be derived to compute the required position of the reflective regions in order to maintain a constant torque during the maneuver. This can be achieved through the formulation of an inverse problem to the derived torque equations.

II. Sail Attitude Control using Continuous Reflectivity Distribution

In this first section, a continuous reflectivity distribution is used to control the planar attitude of a solar sail in low Earth orbit (LEO). In particular, this steering method is applied to counteract the gravity-gradient torques acting on a large rigid sail film. It will be shown that a constant Sun-pointing attitude can be maintained along the orbit, using the proposed chosen concept. A square solar sail film is modeled as a rigid flat Kapton film of density $\delta = 1,572\ \mathrm{kg/m^3}$,[3,4] thickness $d = 2.5 \times 10^{-6}\ \mathrm{m}$ and edge length $L = 50\ \mathrm{m}$, ideally without assembly or payload masses, as shown in figure 1.

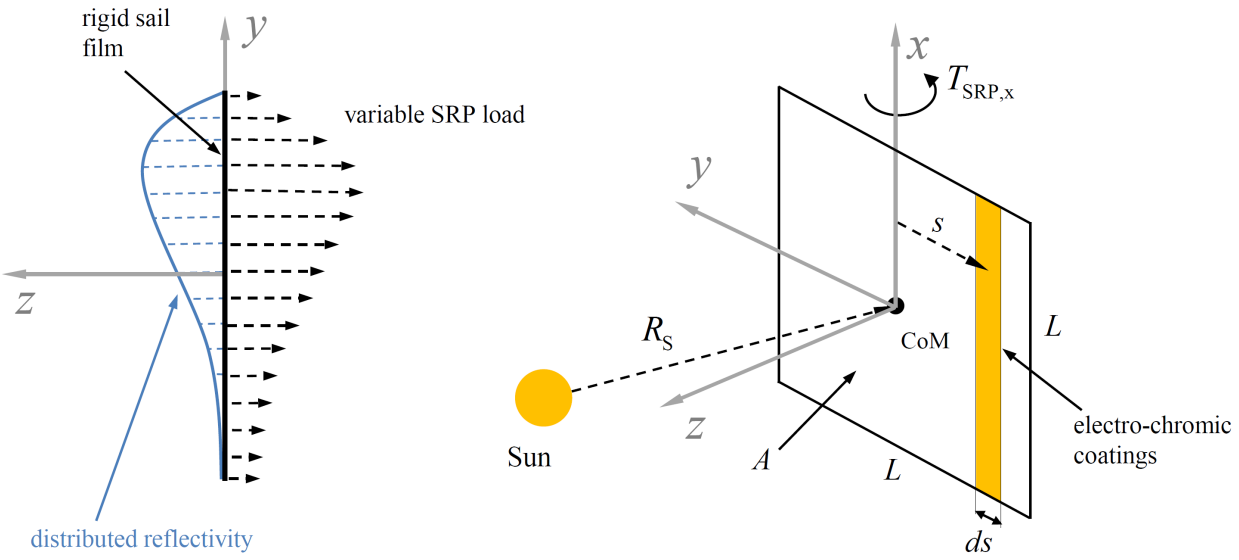

Figure 1. Square solar sail with continuous reflectivity distribution across the surface (left) and sail model using infinitesimal electro-chromic elements (right).

A sail-fixed Cartesian coordinate frame $(\boldsymbol{x}, \boldsymbol{y}, \boldsymbol{z})$ is used to describe the sail attitude along its orbit, where the $\boldsymbol{x}$-axis is constrained to be always perpendicular to the ecliptic plane. This allows only one degree of rotational freedom, while rotation about the sail $\boldsymbol{y}$ and $\boldsymbol{z}$ axes is omitted. The mass moments of inertia of the Kapton film are $I_{xx} = I_{yy} = 2046.9\ \mathrm{kg\,m^2}$ and $I_{zz} = 4093.8\ \mathrm{kg\,m^2}$, with a total mass $m = 9.83\ \mathrm{kg}$. To approximate a continuous reflectivity distribution, it is ideally assumed that the entire sail area A is covered with stripes of infinitesimal electro-chromic coating elements that are able to change their reflectivity in the interval $\rho \in [0, 1]$. The additional mass and thickness of the elements is neglected throughout this preliminary study. When changing the reflectivity of a surface element $dA = L \cdot ds$ on the sail, where s denotes the distance of the element from the axis of rotation $\boldsymbol{x}$, the difference in SRP force creates a torque $T_{\mathrm{SRP,x}}$ about the CoM of the sail. For now, a constant reflectivity is assumed in the element's $\boldsymbol{x}$-direction such

that no torque is generated about the sail $\boldsymbol{y}$-axis. The CoM is assumed to move on a fixed circular LEO of 400 km altitude in the ecliptic plane, as shown in figure 2, while air drag and solar eclipses are ignored for illustration. A constant sail cone angle $\alpha = 0$ deg between the Sun-sail line R_{S} and the sail plane normal is assumed, thus the sail shall be always Sun-pointing along the orbit.

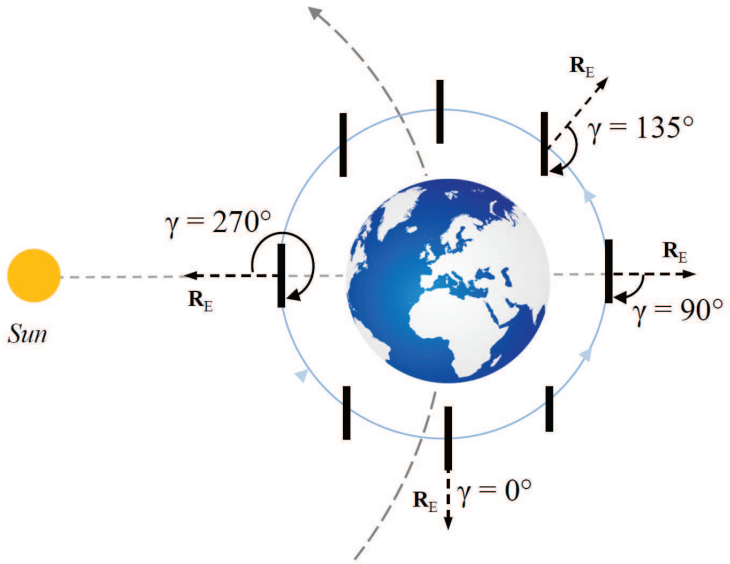

Figure 2. Solar sail on Earth-centered circular LEO of 400 km altitude and constant Sun-pointing attitude.

The gravity-gradient torque along the orbit depends on the angle γ between the sail plane and the Earth radial direction R_{E}. It can be approximated using the standard relation

$$T_{\mathrm{GG,x}} = 3\frac{\mu_E}{R_{\mathrm{CoM}}^3}\sin\gamma\cos\gamma\,(I_{\mathrm{zz}} - I_{\mathrm{yy}}) \tag{1}$$

with μ_E being the Earth's gravitational parameter and R_{CoM} the radial distance of the sail's CoM from the Earth's center.[5] For example, the maximum gravity-gradient torque acting on the sail considered here is of the order $T_{\mathrm{GG,x}} = 4\times10^{-3}$ Nm about the sail $\boldsymbol{x}$-axis. A continuous surface reflectivity distribution $0 \le \rho\,(y) \le 1$ in sail $\boldsymbol{y}$-direction is now assumed to counteract this gravity gradient torque. The SRP force and torque about the sail's CoM are calculated using a simplified SRP model.[1] It assumes that the sail surface is a perfectly (specular) reflecting mirror, neglecting all other forms of optical interactions between the solar photons and the sail surface such as scattering, absorption and thermal re-emission. The model also does not account for wrinkles, and thus assumes a perfectly flat sail surface. Accordingly, the solar radiation pressure p_{SRP} can be written as

$$p_{\mathrm{SRP}} = p_0\,[1+\rho(y)]\left(\frac{R_{S,0}}{R_S}\right)^2\cos^2\alpha \tag{2}$$

at a radial distance R_{S} from the Sun and $p_0 = 4.563\times10^{-6}\mathrm{N/m^2}$ being the solar radiation pressure at $R_{\mathrm{S},0} = 1$ AU. In here, $\rho(y)=1$ represents the ideal mirror that experiences the maximum possible SRP load $p_{\max} = 2p_0$, while the minimum reflectivity $\rho(y)=0$ reduces the effective SRP load to $p_{\max}/2 = p_0$, since only the momentum of the incoming photons is applying a force to the surface. As a consequence, the solar radiation pressure induced forces can be modified directly when changing the surface reflectivity. According to figure 1, the incremental SRP force and torque acting about the CoM on a rectangular sail surface element can now be written as

$$dF_{\mathrm{SRP}} = p_0 L\,[1+\rho(y)]\left(\frac{R_0}{R_{\mathrm{S}}}\right)^2\cos^2\alpha\;ds \tag{3a}$$

$$dT_{\mathrm{SRP,x}} = p_0 Ls\,[1+\rho(y)]\left(\frac{R_0}{R_{\mathrm{S}}}\right)^2\cos^2\alpha\;ds \tag{3b}$$

Assuming a linear reflectivity function in sail $\boldsymbol{y}$-direction

$$\rho(y) = a_0 + a_1\, y \tag{4}$$

the above equations can be integrated over the interval $[-L/2, L/2]$, while constraining the sail surface to be always perpendicular to the Sun-sail line, thus $\alpha = 0$, and assuming that the solar distance $R_{\mathrm{S}} = 1$ AU is constant on the Earth-centered orbit. The resulting SRP force and torque are found to be

$$F_{\mathrm{SRP}} = p_0 L \int_{-L/2}^{L/2} [1 + a_0 + a_1\, y]\, ds \;= p_0 L^2\, [1 + a_0] \tag{5}$$

$$T_{\mathrm{SRP,x}} = p_0 L \int_{-L/2}^{L/2} [1 + a_0 + a_1\, y]\, s ds = \frac{1}{12} p_0 L^4 a_1 \tag{6}$$

It can be seen that the magnitude of the resulting SRP force is only a function of the absolute coefficient a_0. Furthermore, the SRP torque only depends on the slope a_1 of the linear reflectivity function across the film, thus the difference of SRP force on the left and right hand side of the sail. If the forces are equal on both sides ($a_1 = 0$), the torque on the sail is clearly zero, regardless of the absolute value of the SRP force, as determined by a_0. Equation (6) represents the SRP torque that must be generated in order to counteract the gravity-gradient torque $T_{\mathrm{GG,x}}$ along the orbit, thus $T_{\mathrm{SRP,x}}$ must always be equal to $T_{\mathrm{GG,x}}$. Accordingly, the coefficients a_i of the linear reflectivity function $\rho(y)$ can be calculated using the following equations

$$a_1 = \frac{12 T_{\mathrm{GG,x}}}{p_0 L^4}, \qquad\qquad a_0 = \frac{F_{\mathrm{SRP}}}{p_0 L^2} - 1 \tag{7}$$

Although a_1 is always determined through the local $T_{\mathrm{GG,x}}$ that needs to be compensated, a_0 is in principle only constrained by the maximum possible $F_{\mathrm{SRP,\,max}} = 2 p_0 L^2$, for which $a_0 = 1$ and also $\rho(s) = 1 = \mathrm{const}$ across the surface. However, a reflectivity gradient $a_1 \neq 0$ is necessary to create a torque, while at the same time $\rho(y) \leq 1$ must be satisfied across the entire sail. Thus, the upper constraint is $a_{0,\mathrm{max}} < 1$. The lower constraint is determined through the additional condition $\rho(L/2) = 0$ or $\rho(-L/2) = 0$ at the edge of the sail, in order to fix the linear reflectivity curve across the film. Inserting this into the linear reflectivity function, Eq. (4), while keeping a_1 fixed, results in $a_{0,\mathrm{min}} = \pm a_1 L/2$ as the lower limit, depending on the sign of the torque that needs to be created. Figure 3 shows the resulting reflectivity distribution $\rho(y)$ along the film as a

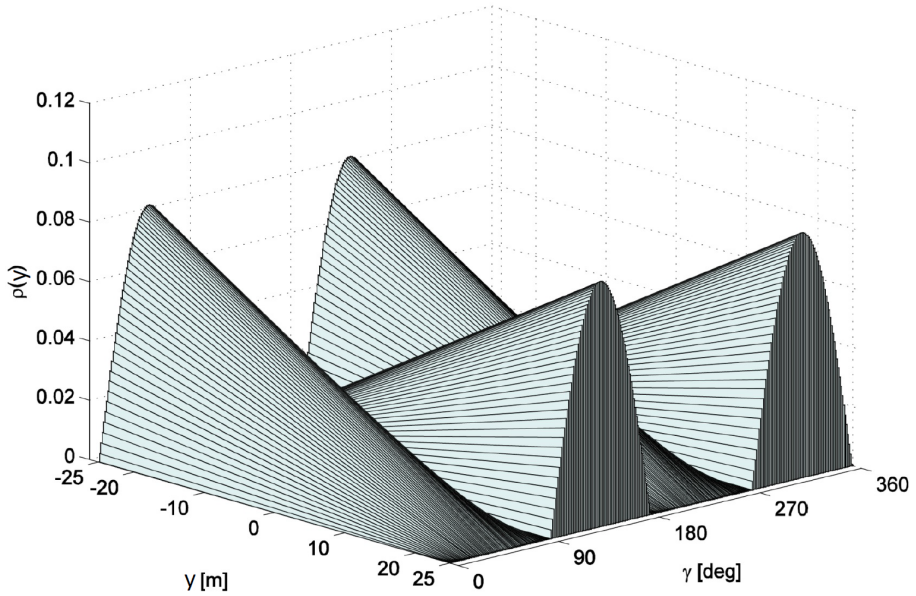

Figure 3. Minimum reflectivity distribution across flat sail film using continuous electro-chromic coating elements.

function of the sail attitude angle γ during one revolution along the orbit for the chosen sail configuration. It can be seen that the necessary reflectivity to balance the gravity-gradient torque is relatively small compared to the maximum reflectivity that can be achieved with currently developed electro-chromic devices, e.g. as used on the IKAROS solar sail.[6] According to the reference, a maximum $\rho_{\max} = 0.6$ is currently possible. Accordingly, for the chosen application to counteract gravity gradient torques, the optical steering method has not reached its full potential. The maximum control torque that can be achieved for the current sail, assuming that one half of the sail is set to $\rho = 1$, while $\rho = 0$ for the other half, is $T_{\mathrm{SRP,x}} = 0.143$ Nm, thus 35 times higher than the maximum gravity gradient torque in LEO.

III. Sail Attitude Control using Discrete Reflectivity Regions

In the following, we further demonstrate two-axis attitude control using discrete reflectivity regions on the surface. Instead of varying ρ in the interval $[0, 1]$, as shown in section II, the electro-chromic coatings are now restricted between two states, either 'on' ($\rho_{\max} = 1$) or 'off' ($\rho_{\min} = 0$). This is achieved by introducing a boundary line between the 'on' and 'off' states, used to separate regions of high and low reflectivity, as shown in figure 4. When distributing controlled regions of high and low reflectivity across the surface, a wide range of torques can be generated in the sail-plane, however, torques perpendicular to the surface are not possible.

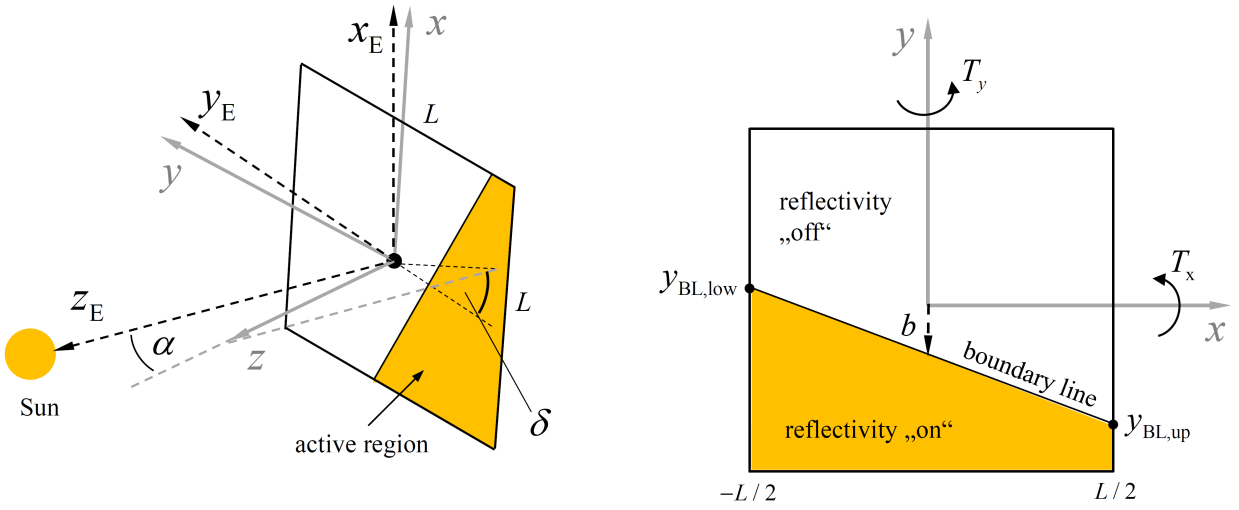

Figure 4. Square solar sail with discrete reflectivity region controlled by moving a boundary line between two states, 'on' (specular reflection) and 'off' (diffuse reflection), and torques created about the in-plane sail axes

The on/off boundary-line is described through a linear function

$$y_{\mathrm{BL}}(x) = ax + b \tag{8}$$

in the $(\boldsymbol{xy})$-plane of the sail, with an arbitrary slope coefficient a and offset coefficient b, describing its vertical offset from the sail $\boldsymbol{x}$-axis. Furthermore, two geometrically mirrored on/off cases can be chosen for the electro-chromic coatings above and below the boundary line, as shown in figure 5. The first case represents an active reflectivity above the boundary-line and inactive below (further named as the 'upper case'), or vice versa, the second case indicates reflectivity 'off' above y_{BL} and 'on' below (named as the 'lower case'). Switching between the two cases only changes the sign of the torques, not their magnitude. The SRP torques now depend on the two coefficients a and b, the local cone angle α (i.e. the current sail attitude), and the considered on/off case.

In $\boldsymbol{x}$ and $\boldsymbol{y}$-components, the SRP torques at 1 AU solar distance are now written

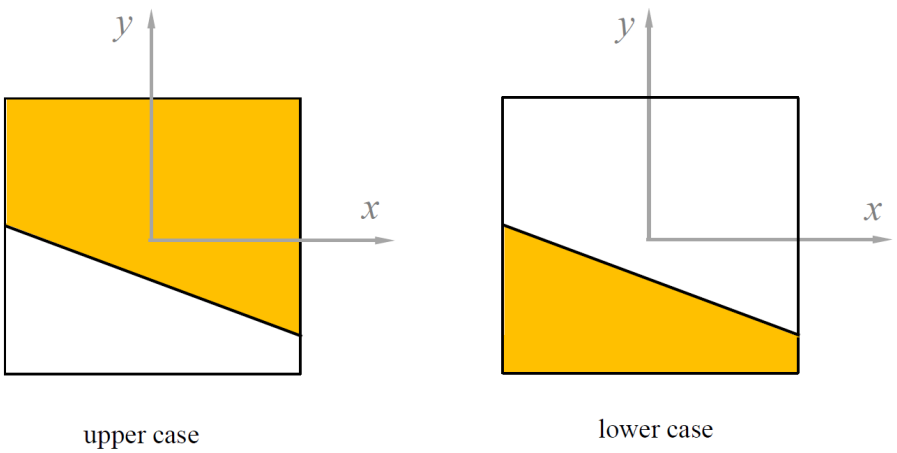

Figure 5. Possible on/off cases for the two reflectivity regions on the surface, separated by the reflectivity boundary-line

$$\boldsymbol{T}_{\mathrm{x}} = -p_0 \cos^2\alpha \int_{-L/2}^{L/2} \int_{ax+b}^{L/2} y \,\mathrm{dydx}\, \boldsymbol{x} \tag{9a}$$

$$\boldsymbol{T}_{\mathrm{y}} = \quad p_0 \cos^2\alpha \int_{-L/2}^{L/2} \int_{ax+b}^{L/2} x \,\mathrm{dydx}\, \boldsymbol{y} \tag{9b}$$

when assuming the 'upper case', thus only the electro-chromic coatings above the boundary-line are active. When the RCDs are switched into the 'lower case', the limits of the inner integral in $\boldsymbol{y}$-direction need to be inverted to $[-L/2, ax+b]$, cf. figure 4, which is equivalent to changing the signs of the torques. As mentiones above, when using this attitude control concept, no torques about the sail **z**-axis, normal to the surface, can be generated.

When integrating equation (9), seven torque cases have to be considered separately, depending on the chosen reflectivity-line coefficients and thus, on the shape of the active region on the sail surface. Each case is defined through the intersection of the reflectivity-line with the integration limits in $\boldsymbol{x}$-direction, as can be seen in figure 6. Accordingly, the following conditionals are introduced at the edges of the sail surface

$$y_{\mathrm{BL,low}} = -a\left(\frac{L}{2}\right) + b \lessgtr \pm\frac{L}{2} \tag{10a}$$

$$y_{\mathrm{BL,up}} = \quad a\left(\frac{L}{2}\right) + b \lessgtr \pm\frac{L}{2} \tag{10b}$$

For example, if the coefficients of the boundary-line are chosen so that $-L/2 \leq y_{\mathrm{BL,low}} \leq L/2$ and $-L/2 \leq y_{\mathrm{BL,up}} \leq L/2$, the resulting torques are of the type 'case 1', as shown in figure 6. After defining all seven cases accordingly, analytic expressions for the sail torques can be found. In particular, a set of boundary equations for a and b can be introduced to identify the torque case from a given reflectivity-line. As a result, the sail torques are now fully determined by the following conditional scheme, given here for the 'upper case', when the sail region above the reflectivity-line is activated

Case 1 $\quad a \geq 0 \ \wedge\ L/2(a-1) \leq b \leq L/2(1-a) \quad$ or $\quad a \leq 0 \ \wedge\ -L/2(a+1) \leq b \leq L/2(a+1)$

$$\boldsymbol{T}_{\mathrm{x,upper}} = \quad p_0 L^3 \cos^2\alpha \left[\frac{1}{2}\frac{b^2}{L^2} - \frac{1}{8} + \frac{1}{24}a^2\right] \boldsymbol{x} \tag{11a}$$

$$\boldsymbol{T}_{\mathrm{y,upper}} = \frac{1}{12} p_0 a L^3 \cos^2\alpha \, \boldsymbol{y} \tag{11b}$$

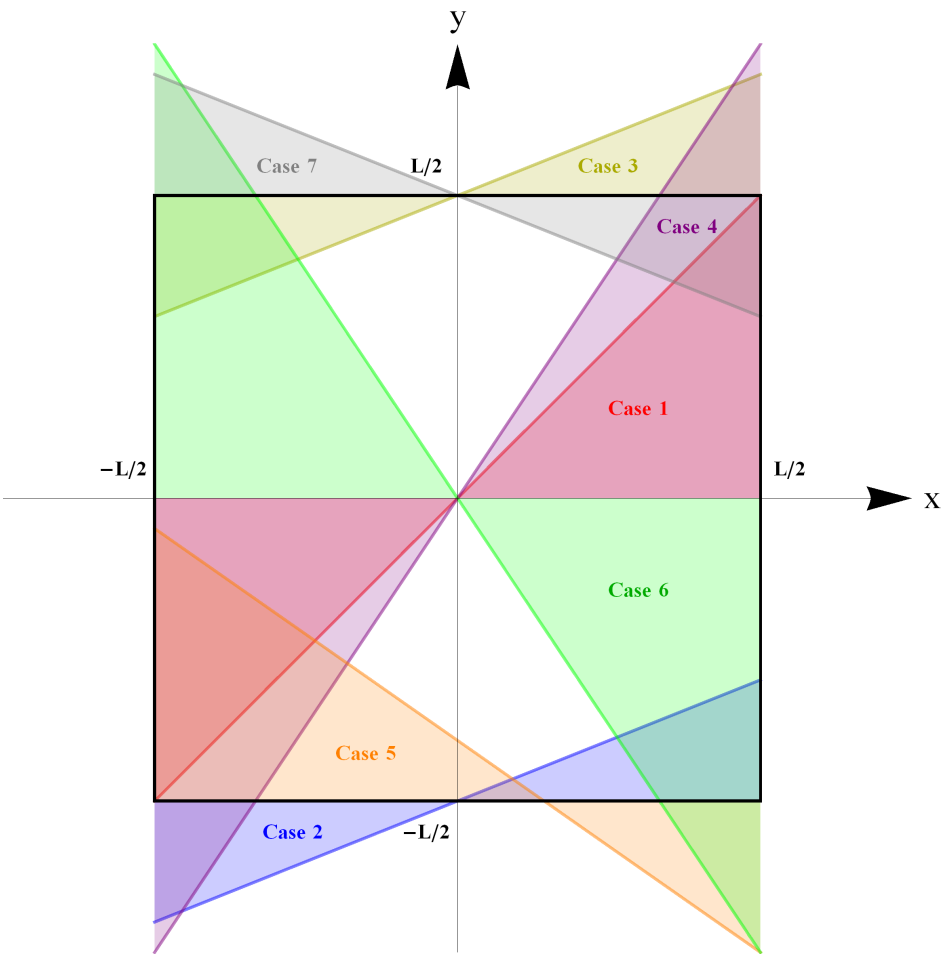

Figure 6. Torque cases depending on the position of the boundary-line between specular and diffuse reflection on the sail surface

Case 2 $a > 0 \ \wedge \ -L/2(a+1) < b < L/2(1-a) \ \wedge \ b < L/2(a-1)$

$$\boldsymbol{T}_{\mathrm{x,upper}} = p_0 L^3 \cos^2\alpha \left[\frac{1}{6}\frac{b^3}{aL^3} + \frac{1}{4}\frac{b^2}{L^2} - \frac{1}{8}\frac{b}{aL} + \frac{1}{8}\frac{ab}{L} - \frac{1}{16} - \frac{1}{24}\frac{1}{a} + \frac{1}{48}a^2\right]\boldsymbol{x} \tag{12a}$$

$$\boldsymbol{T}_{\mathrm{y,upper}} = p_0 L^3 \cos^2\alpha \left[\frac{1}{6}\frac{b^3}{a^2L^3} + \frac{1}{4}\frac{b^2}{a^2L^2} - \frac{1}{8}\frac{b}{L} + \frac{1}{8}\frac{b}{a^2L} - \frac{1}{16} - \frac{1}{24}a + \frac{1}{48}\frac{1}{a^2}\right]\boldsymbol{y} \tag{12b}$$

and the other cases can be derived in a similar way. Switching from the 'upper case' to the 'lower case' changes signs in the previous equations such as $\boldsymbol{T}_{\mathrm{x,lower}} = -\boldsymbol{T}_{\mathrm{x,upper}}$ and $\boldsymbol{T}_{\mathrm{y,lower}} = -\boldsymbol{T}_{\mathrm{y,upper}}$.

In order to demonstrate the concept, a sample square sail configuration, with edge length $L = 100\,\mathrm{m}$ and total mass $m = 200\,\mathrm{kg}$, is now considered. The sail is ideally assumed to be rigid, with mass moments of inertia $I_{\mathrm{xx}} = I_{\mathrm{yy}} = 1.67 \times 10^5\ \mathrm{kg\,m^2}$ and $I_{zz} = 3.34 \times 10^5\ \mathrm{kg\,m^2}$. The achievable torques as a function of the reflectivity-line coefficients a, b and for increasing cone angle are shown in figure 7, with the electro-chromic elements activated in the 'lower case'. As can be seen, this activation case creates a positive T_{x} over the entire (a, b) domain, while the magnitude decreases for increasing cone angle. The maximum torque is created for $(a, b) = (0, 0)$, when all electro-chromic coatings on the lower half of the sail are active. In

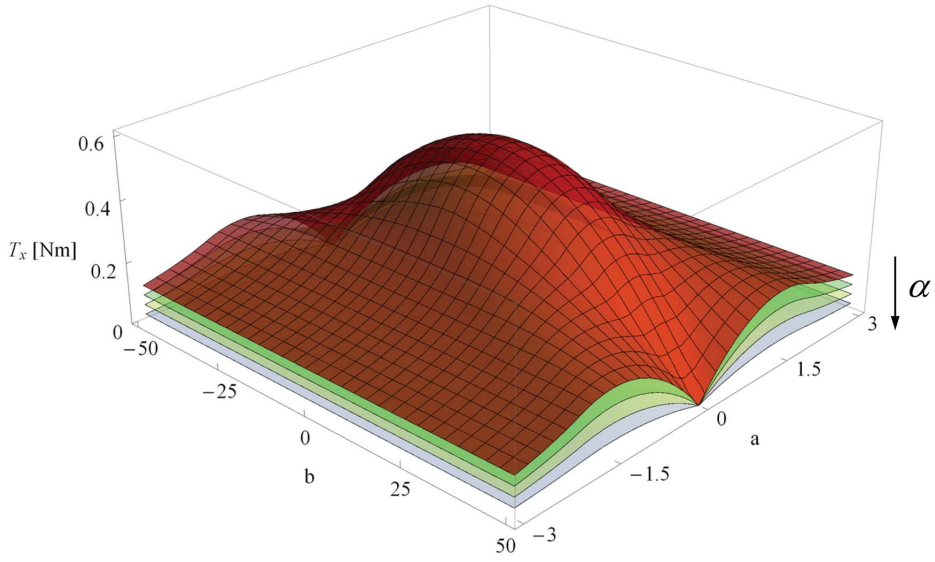

(a) Torque in sail x-direction

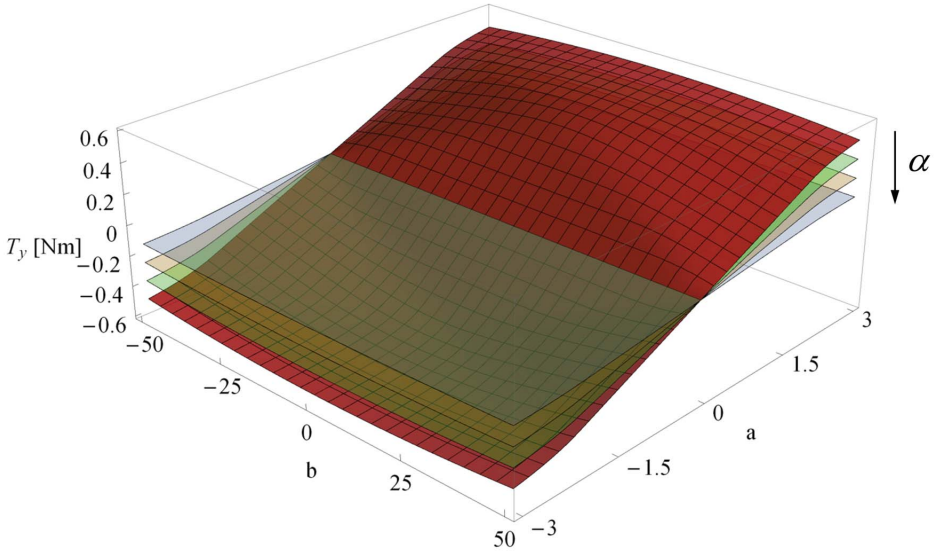

(b) Torque in sail y-direction

Figure 7. In-plane sail torques over reflectivity-line coefficients a and b and as function of sail cone angle α. Reflectivity regions activated in 'lower case'

$\boldsymbol{y}$-direction, the achievable torques mainly depend on the slope a of the reflectivity-line and only to a very limited extent on the coefficient b. In addition, also negative torques can be created, which is not possible in the $\boldsymbol{x}$-direction for the selected 'lower case'. The maximum torques about both sail axes are found to be $T_{\mathrm{max,x}} = T_{\mathrm{max,y}} = \pm 0.57$ Nm,which occurs when all coating elements on one half of the sail are active. For example, applying this torque on the given sample sail results in a full rotation of 360 deg in approx. 1900 s $\approx$ 32 min.

All seven torque cases over the selected (a, b)-domain are visible in figure 8 through the use of colored regions, showing both torque components for a sail cone angle of $\alpha = 0$ deg and an active 'upper case' reflectivity distribution. The solid lines indicate T_{x} and the dashed lines indicate T_{y}. From the figure, the

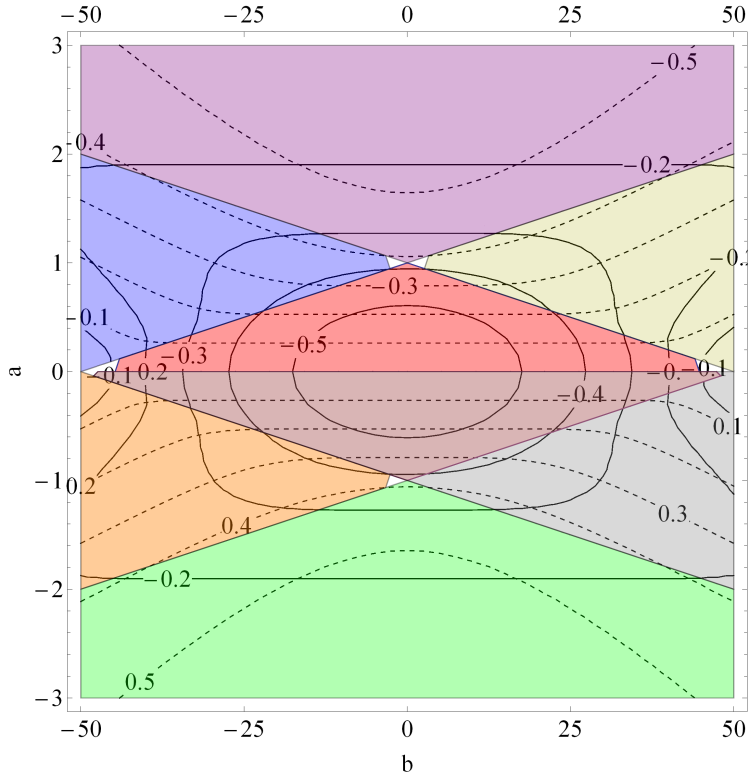

Figure 8. In-plane Sail torques $\mathbf{T_x}$ (solid lines) and $\mathbf{T_y}$ (dashed lines) as function of reflectivity-line coefficients a and b and sail cone angle $\alpha = 0$ deg, with colored regions indicating the torque case. Discrete reflectivity regions are activated in 'upper case'

feasible torques for each chosen reflectivity line in terms of a and b can be obtained. It is visible that no arbitrary torques about both sail axis can be generated, even when staying below T_{max} for a chosen sail configuration.

A. Sail Attitude Maneuvers using Discrete Reflectivity

The described attitude control concept of employing discrete reflectivity regions across the sail surface is now applied to change the attitude of a sail in a Sun-centered orbit from a chosen initial attitude towards Sun-pointing, using combined torques T_{x} and T_{y} in the sail plane. The attitude dynamics of the sail are described using Euler's Equation in quaternion notation.[5,7] In the present analysis, it is assumed that attitude changes are not affecting the sail's Sun-centered orbit, thus the orbit and attitude motion are decoupled. Choosing quaternions for attitude representation is beneficial compared to other attitude descriptors such as Euler angles, since quaternions have one redundant parameter (no singularities) and offer a lower computational effort (no trigonometric functions).[8,9] Accordingly, the governing differential equation system (DES) of the rotational motion of a rigid body can be written as

$$\dot{\bar{q}} = \frac{1}{2}\, \bar{q} \otimes \bar{\omega} \tag{13}$$

representing the first derivative of the attitude quaternion $\bar{q}$ due to the sail's angular velocity $\bar{\omega}$. Furthermore, the second derivative of the quaternion due to an external torque $\boldsymbol{T}$ about the body axes follows as

$$\ddot{\bar{q}} = \dot{\bar{q}} \otimes \bar{q}^{-1} \otimes \dot{\bar{q}} + \frac{1}{2}\,\bar{q} \otimes \dot{\bar{\omega}} \quad \text{with } \dot{\bar{\omega}} = \begin{pmatrix} 0 \\ [I]^{-1}(\boldsymbol{T} - \boldsymbol{\omega} \times [I]\boldsymbol{\omega}) \end{pmatrix} \tag{14}$$

with $[I]$ the mass moments of inertia tensor and $\otimes$ representing the quaternion product.[8] The upper $(\bar{})$ denotes a quaternion vector

$$\bar{q} = q_1 + \boldsymbol{q} = \cos\left(\frac{\theta}{2}\right) + \boldsymbol{a} \cdot \sin\left(\frac{\theta}{2}\right) \tag{15}$$

with rotation angle θ and axis of rotation $\boldsymbol{a}$ with respect to a defined reference frame. Throughout this work, the so called ecliptic reference frame $(\boldsymbol{x}_\mathrm{E}, \boldsymbol{y}_\mathrm{E}, \boldsymbol{z}_\mathrm{E})$ is used, centered in the sail's CoM, as can be seen in figure 4. The $\boldsymbol{z}_\mathrm{E}$ axis is oriented towards the Sun, the $\boldsymbol{y}_\mathrm{E}$ component is always in the ecliptic plane of the sail's Sun-centered orbit, and $\boldsymbol{x}_\mathrm{E}$ completes the right-handed coordinate system.

The above DES represents a system of second order differential equations and is formulated as an initial value problem of the form

$$\ddot{\bar{q}} = \mathrm{f}\big(\dot{\bar{q}}, \bar{q}, \dot{\bar{\omega}}, t\big), \quad \bar{q}(t = t_0) = \bar{q}_0, \quad \dot{\bar{q}}(t = t_0) = \dot{\bar{q}}_0, \quad \dot{\bar{\omega}}(t = t_0) = \dot{\bar{\omega}}_0 \tag{16}$$

The system is solved using a Runge-Kutta Nyström (RKN) integration scheme.[10] A constant torque will be used to rotate the sail from its initial to final attitude (bang-bang control). Halfway during the maneuver, when the sail attitude has rotated over an angle $\theta/2$, the sign of the torque is inverted to decelerate the motion until the final attitude is reached. After selecting the required sail torques $(T_\mathrm{x}, T_\mathrm{y})_\mathrm{req}$, the corresponding reflectivity-line coefficients as a function of current sail attitude can be found through the formulation of an inverse problem approach.

B. Inverse Problem Approach for Reflectivity-Line Control

When re-writing the torque equation (11) and (12) for the coefficients a and b, the reflectivity-line can be expressed as a function of the (required) torques and the current cone angle α. Given here for torque case 1 only, the inverse problem results in

Case 1 $\quad a \geq 0 \ \wedge \ L/2(a-1) \leq b \leq L/2(1-a)$

$$a = -12\frac{T_\mathrm{y,upper}}{p_0 L^3 \cos^2\alpha} \tag{17a}$$

$$b = \pm\frac{L}{2}\sqrt{1 + \frac{8T_\mathrm{x,upper}}{p_0 L^3 \cos^2\alpha} - \frac{48T_\mathrm{y,upper}^2}{(p_0 L^3)^2 \cos^4\alpha}} \tag{17b}$$

with the following conditions on the two torque components

$$-\frac{1}{12}p_0 L^3 \cos^2\alpha \leq T_\mathrm{y,upper} \leq 0 \tag{18a}$$

$$-\frac{1}{8}\left(L^3\cos^2\alpha - \frac{48\,T_\mathrm{y,upper}^2}{p_0 L^3 \cos^2\alpha}\right) \leq T_\mathrm{x,upper} \leq 3T_\mathrm{y,upper} + \frac{24\,T_\mathrm{y,upper}^2}{p_0 L^3 \cos^2\alpha} \tag{18b}$$

and for an active 'upper case' reflectivity distribution. Consequently, after selecting the required torques that satisfy the maximum achievable limits for a given sail and the previous conditions of equation 18, the shape and position of the reflectivity-line in order to create these torques can now be found for a sail attitude towards the Sun, or cone angle, respectively.

C. Sample Sail Attitude Maneuver

The inverse problem solution is now applied to perform a basic sail maneuver. Initially, the sail is chosen to be tilted over a cone angle $\alpha_{\text{init}} = 40$ deg and clock angle $\delta_{\text{init}} = 52$ deg, as shown in figure 9. This translates into a rotation angle $\theta_x = 38$ deg and $\theta_y = 12$ deg about the sail $\boldsymbol{x}$ and $\boldsymbol{y}$-axis. After the maneuver, the sail shall be Sun-pointing, thus $\alpha_{\text{final}} = 0$. From the quaternion approach, it follows that the axis of rotation is $\boldsymbol{a} = (-0.3, -0.1, 0)$. This axis can be obtained from the initial attitude quaternion that is calculated from the initial displacement angles θ_x and θ_y. Therefore, a constant torque couple of $T_{\text{x}} = -0.3$ Nm and $T_{\text{y}} = -0.1$ Nm is selected so that the total torque vector matches the initial displacement of the sail with respect to the ecliptic reference frame. Since the torque T_{x} is negative, the 'upper case' distribution needs to be used, as it was shown in figure 8.

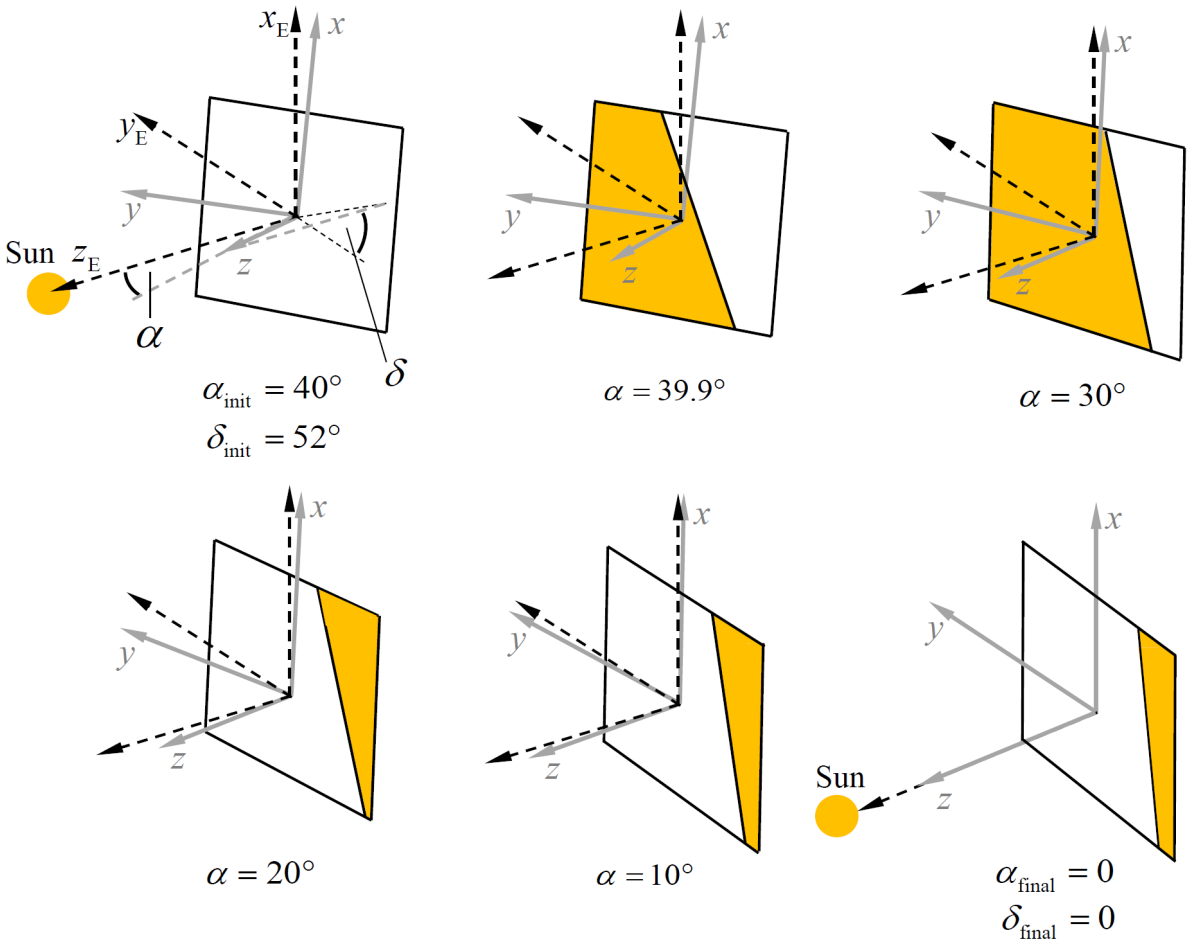

Figure 9. Maneuver sequence for selected initial sail attitude $\alpha_{\text{init}} = 40$ deg and clock angle $\delta_{\text{init}} = 52$ deg towards final Sun-pointing attitude

For the selected initial cone angle, the achievable torques over the (a, b)-domain of the reflectivity-line are visible in figure 10, for an active 'upper case' reflectivity distribution. The solid lines again indicate T_{x} and the dashed lines indicate T_{y}. Red points identify the two feasible (a, b)-sets for the selected torques, as calculated from the inverse problem in section III B. They both require the same slope of the reflectivity-line, however, a positive or negative offset in $\boldsymbol{y}$-direction can be chosen. Furthermore, from Equation (17) of the inverse problem, the reflectivity-line coefficients are now fully determined as a function of the local cone angle during the maneuver, as shown in figure 11. When adapting the reflective region across the surface during the maneuver according to the derived control law for the reflectivity-line, the in-plane torques acting on the sail can be kept constant, although the light incidence angle (cone angle) and thus the SRP forces are varying during the rotation. The sail attitude is now computed through the DES of rotational motion, equation (14), using the integration method described in equation (16). The resulting time history of the cone angle and

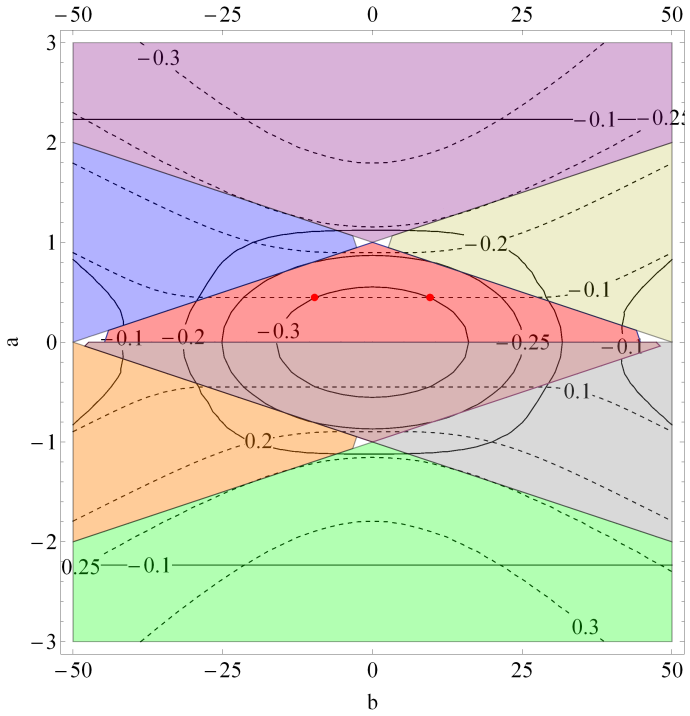

Figure 10. In-plane sail torques T_x (solid lines) and T_y (dashed lines) as function of reflectivity-line coefficients a and b and sail cone angle $\alpha = 40$ deg. Red dots indicate feasible sets $(a, b) = (0.45, \pm 9.59)$ for the required maneuver torques. Discrete reflectivity regions are activated in 'upper case'

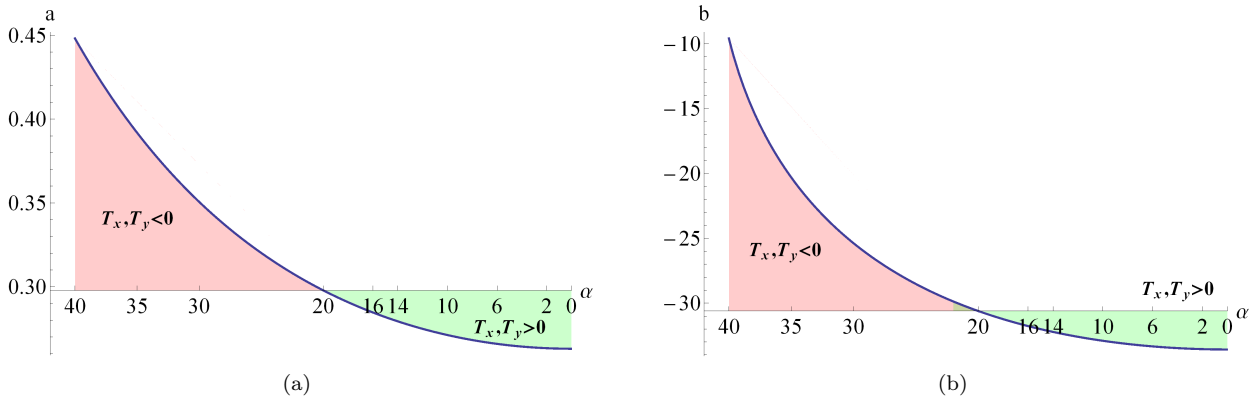

Figure 11. Controlled reflectivity-line coefficients a and b as function of sail cone angle α for selected maneuver towards Sun-pointing attitude

angular rates ω_x and ω_y of the sail about the in-plane body axes are shown in figure 12, together with the applied bang-bang torque profile. The total maneuver time to rotate the sail into Sun-pointing attitude is 1216 s $\approx$ 20 min.

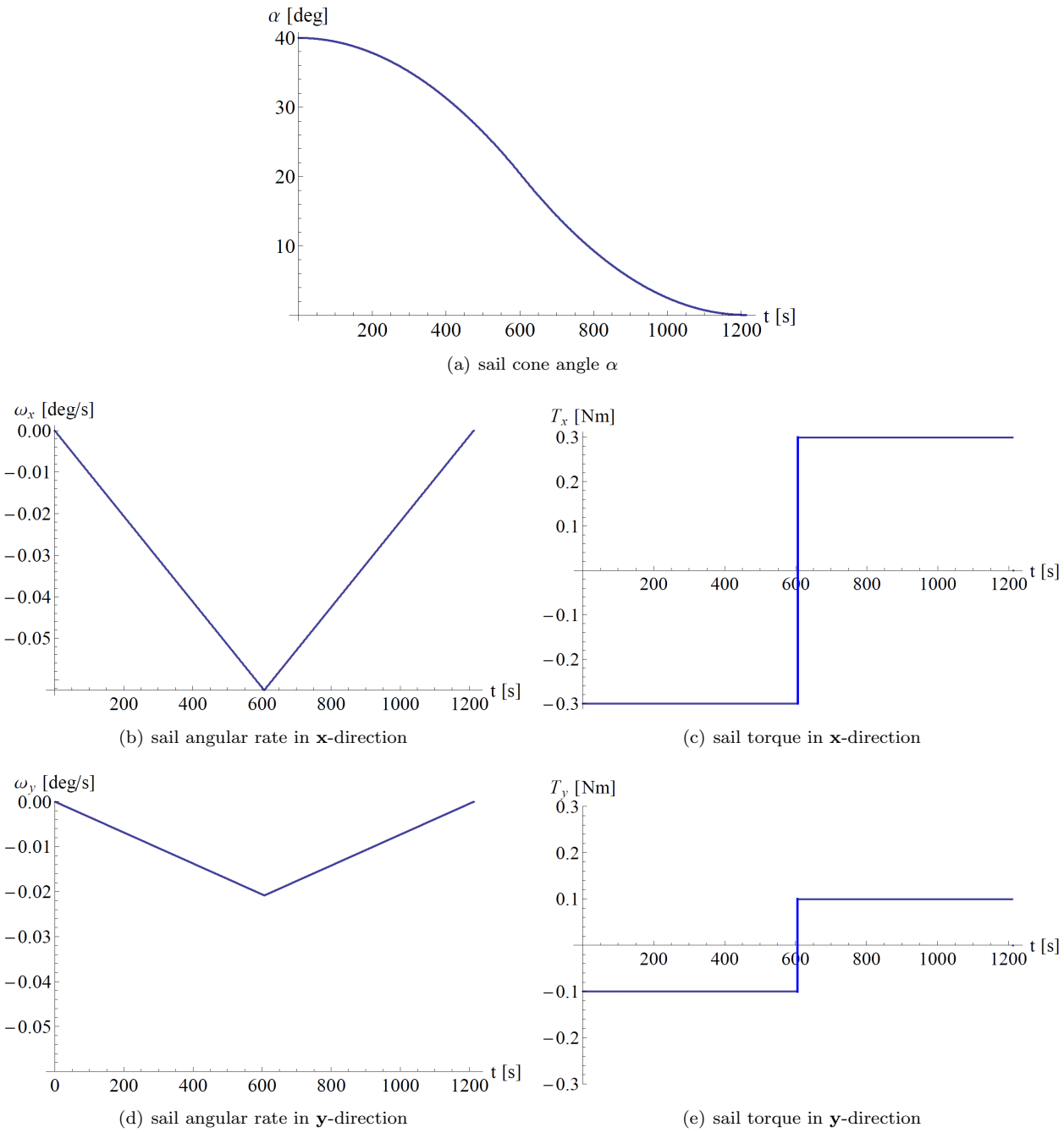

(a) sail cone angle α

(b) sail angular rate in **x**-direction

(c) sail torque in **x**-direction

(d) sail angular rate in **y**-direction

(e) sail torque in **y**-direction

Figure 12. Sail maneuver time-history towards final Sun-pointing attitude

IV. Conclusions

A variable reflectivity distribution across the surface of a solar sail film has been proposed to investigate flexible steering for solar sails without the use of mechanical systems. The surface reflectivity can be manipulated when distributing electro-chromic elements across the sail film that change their reflectivity according to an applied electric potential. First, a continuous linear reflectivity function was employed to control the attitude of the sail in low Earth orbit under the influence of gravity-gradient torques. It was shown that a constant Sun-pointing attitude can be maintained along the orbit, while only a very low value of the reflectivity is needed. This is beneficial, since currently developed electro-chromic coatings are not yet capable of adapting their optical properties arbitrarily between diffuse and fully specular reflection.

Furthermore, a discrete concept using controlled regions of active reflectivity across the surface has been employed to enable two-axis attitude control of a solar sail. When controlling the boundary-line between two regions of specular and diffuse reflection, a wide range of in-plane torque-vector directions can be generated, depending on the shape and position of the boundary-line on the surface. Since the torque magnitude depends on the light incidence angle between the sail and the Sun, an analytic control law has been derived that maintains a constant torque even when the sail is rotating during maneuver phases. The control law moves the boundary-line across the surface, depending on the current sail attitude with respect to the Sun. The concept has been demonstrated by maneuvering the sail from its initial attitude towards Sun-pointing. The proposed concepts introduce a more flexible and potentially lightweight attitude control method to large gossamer spacecraft and hereby represent major opportunities for future highly-integrated 'smart' spacecraft with on-board autonomy.

Acknowledgments

This work was funded by the European Research Council Advanced Investigator Grant - 227571: VISIONSPACE: Orbital Dynamics at Extremes of Spacecraft Length-Scale.

References

[1]McInnes, C. R., *Solar Sailing: Technology, Dynamics and Mission Applications*, Springer-Praxis Series in Space Science and Technology, Springer-Verlag, Berlin, 1999, pp. 1–55.

[2]Demiryont, H. and Moorehead, D., "Electrochromic Emissivity Modulator for Spacecraft Thermal Management," *Solar Energy Materials and Solar Cells*, Vol. 93, No. 12, 2009, pp. 2075–2078.

[3]Sleight, D. W. and Muheim, D. M., "Parametric studies of square solar sails using finite element analysis," *Collect. of Pap. - 45th AIAA/ASME/ASCE/AHS/ASC Struct., Struct. Dyn. and Mater. Conf.; 12th AIAA/ASME/AHS Adapt. Struct. Conf.; 6th AIAA Non-Deterministic Approaches Forum; 5th AIAA Gossamer Spacecraft Forum, April 19, 2004 - April 22, 2004*, Vol. 1 of *Collection of Technical Papers - AIAA/ASME/ASCE/AHS/ASC Structures, Structural Dynamics and Materials Conference*, American Inst. Aeronautics and Astronautics Inc., 2004, pp. 85–97.

[4]DuPont, "Kapton Technical Data Sheet," DuPont High Performance Films, Retrieved 5 November 2013, "http://www2.dupont.com/Kapton/en_US/assets/downloads/pdf/HN_datasheet.pdf".

[5]Schaub, H., *Analytical Mechanics of Space Systems, 2nd Edition*, AIAA Educational Series, 2009.

[6]Funase, R., Mori, O., Tsuda, Y., Shirasawa, Y., Saiki, T., Mimasu, Y., and Kawaguchi, J., "Attitude control of IKAROS solar sail spacecraft and its flight results," *61st International Astronautical Congress 2010, IAC 2010, September 27, 2010 - October 1, 2010*, Vol. 6, International Astronautical Federation, IAF, pp. 4720–4725.

[7]Borggräfe, A., *Analysis of Interplanetary Solar Sail Trajectories with Attitude Dynamics*, Master Thesis, Institute of Flight System Dynamics, RWTH Aachen University, 2011.

[8]Kuipers, J., *Quaternions and Rotation Sequences*, Princeton University Press, 1999.

[9]Hanson, A., *Visualizing Quaternions*, Morgan Kaufmann, 2006.

[10]Bettis, D., *A Runge-Kutta Nyström Algorithm*, Celestial Mechanics 8, Kluwer Academic Publishers, 1973.